



# Temperature dependent photoluminescence of $\text{Cr}^{3+}$ doped $\text{Sr}_8\text{MgLa}(\text{PO}_4)_7$

Beata Malysa<sup>a,b,\*</sup>, Andries Meijerink<sup>b,\*\*</sup>, Thomas Jüstel<sup>a</sup>

<sup>a</sup> Münster University of Applied Sciences, Stegerwaldstrasse 39, D-48565, Steinfurt, Germany

<sup>b</sup> University Utrecht, Princetonplein 1, NL-3584, Utrecht, the Netherlands

## ARTICLE INFO

### Keywords:

Thermal quenching  
 $\text{Cr}^{3+}$  photoluminescence  
 Broad band NIR emission  
 Ortho-phosphates  
 Phosphor converted LEDs  
 NIR light sources

## ABSTRACT

Broad band near infrared (NIR) light sources are currently of great interest in many application areas, especially in near infrared spectroscopy (NIRS). Due to the declining availability of incandescent and halogen light sources, there is a strong demand for other efficient broad band NIR light sources. NIR phosphor converted (pc) LEDs are presently explored to realize efficient broadband NIR sources. Herein, we report on the luminescence properties of  $\text{Cr}^{3+}$  doped  $\text{Sr}_8\text{MgLa}(\text{PO}_4)_7$  (SMLP) which is a potential luminescent converter for high power broad band NIR pcLEDs. Microcrystalline powders of SMLP doped with different  $\text{Cr}^{3+}$  concentration were synthesized by solid state reactions and exhibit efficient near infrared broad band emission upon excitation in the blue/cyan spectral range. The emission extends from 700 to 1000 nm (FWHM = 140 nm) and is assigned to the spin-allowed  $^4\text{T}_2 \rightarrow ^4\text{A}_2$  transition of  $\text{Cr}^{3+}$ . The optical properties of  $\text{Cr}^{3+}$  ions in SMLP were examined in terms of spectroscopic parameters such as crystal field strength, Racah parameters, and phonon coupling parameters. The photoluminescence quenching temperature ( $T_{1/2}$ ) is a crucial parameter for blue to NIR radiation converters as the high power (In,Ga)N LEDs (pumping source) reach junction temperatures up to  $\sim 450$  K. The  $\text{Sr}_8\text{MgLa}(\text{PO}_4)_7:\text{Cr}^{3+}$  phosphors reveal rather low quenching temperatures ( $T_{1/2} \cong 300$  K) mainly due to a strong electron-phonon coupling, while the presented results provide insight in factors determining thermal quenching.

## 1. Introduction

The increasing demand for improvement of product quality and monitoring system in industry has led to a gradual replacement of time-consuming conventional analytical techniques by more specific, compatible, and reliable analytical methods based on near infrared spectroscopy [1]. Recently, NIR spectroscopy has become very important as a non-invasive and rapid analytical tool, e.g., in agriculture, food engineering, and pharmaceutical and biomedical science [2,3].

Commonly used NIR light sources for NIRS are incandescent lamps and NIR LEDs based on (Al,Ga)As semiconductor chip. The traditional tungsten and halogen lamps have a broadband spectrum extending from the UV to infrared range, but their low efficiency, short lifetime, high bulb temperature and large size limit the use of these light sources, e.g., in hand-held devices [4]. The NIR LEDs possess some advantages over tungsten-halogen lamps, i.e. higher electrical to optical conversion efficiency (wall-plug efficiency  $\sim 50\%$ ), longer lifetime ( $\sim 100\,000$  h), and much smaller size [5]. However, a severe drawback of NIR LEDs is the relatively narrow band emission spectrum (spectral bandwidth at 50% of maximum intensity  $\sim 30$  nm), and sensitivity to temperature and drive current in terms of intensity and peak wavelength [6,7].

A promising strategy to overcome the limitations of commercial broad band NIR light sources is the use of an efficient high power blue LED in combination with a suitable broad band NIR emitting phosphor [8,9]. In view of the increased interest in NIR phosphor converted LEDs, the demand for novel NIR emitting phosphors for solid state lighting is growing [10]. To realize high power broad band NIR phosphor converted LEDs with superior performance efficient radiation converters with high thermal stability, i.e. high quenching temperature ( $T_{1/2} > 450$  K) are required.

$\text{Cr}^{3+}$  doped materials are very promising downshifters for NIR pcLEDs exhibiting a broad band emission in the NIR spectral range upon blue light excitation. Due to a rather high sensitivity of the optical properties of  $\text{Cr}^{3+}$  ions to the local surroundings, the  $\text{Cr}^{3+}$  emission can be tuned from a narrow R-line emission ( $^2\text{E} \rightarrow ^4\text{A}_2$ ) in a strong crystal field to a broad band emission ( $^4\text{T}_2 \rightarrow ^4\text{A}_2$ ) in a weak crystal field.

Recently,  $\text{Sr}_8\text{MgRE}(\text{PO}_4)_7$  (RE = La, Gd, Lu, Sc, Y) ortho-phosphates have attracted considerable attention as hosts for the design of new LED phosphors types. C.-H. Huang et al. have developed a novel yellow emitting  $\text{Sr}_8\text{MgGd}(\text{PO}_4)_7:\text{Eu}^{2+}$  phosphor for warm white pcLEDs, whereas Z. Zheng reported on an efficient and blue to red adjustable emission of  $\text{SMLP}:\text{Ce}^{3+}, \text{Eu}^{2+}, \text{Mn}^{2+}$  [11,12].  $\text{Sr}_8\text{MgLa}(\text{PO}_4)_7$  host has a

\* Corresponding author. Münster University of Applied Sciences, Stegerwaldstrasse 39, D-48565, Steinfurt, Germany.

\*\* Corresponding author.

E-mail addresses: [beata.malysa@fh-muenster.de](mailto:beata.malysa@fh-muenster.de) (B. Malysa), [a.meijerink@uu.nl](mailto:a.meijerink@uu.nl) (A. Meijerink), [tj@fh-muenster.de](mailto:tj@fh-muenster.de) (T. Jüstel).

rigid crystal structure and thus exhibits high chemical and thermal stability. To the best of our knowledge, there are no reports on the optical properties of  $\text{Cr}^{3+}$  in  $\text{Sr}_8\text{MgLa}(\text{PO}_4)_7$ , which is a suitable host lattice for the incorporation of  $\text{Cr}^{3+}$  ions onto  $\text{Mg}^{2+}$  octahedral sites. Herein, we report on the NIR broad band emission spectra of  $\text{Cr}^{3+}$  in SMLP and the influence of temperature and chromium concentration on the optical properties.

## 2. Experimental section

The microcrystalline powders of  $\text{Sr}_8\text{MgLa}(\text{PO}_4)_7$  doped with  $\text{Cr}^{3+}$  were synthesized by solid state reaction in air. As starting materials  $\text{SrCO}_3$  (Treibacher Industrie AG, 99.99%),  $\text{MgO}$  (Alfa Aesar, 99.95%),  $\text{La}_2\text{O}_3$  (Treibacher Industrie AG, 99.995%),  $\text{NH}_4\text{H}_2\text{PO}_4$  (Merck KGaA, 99.0%), and  $\text{Cr}_2\text{O}_3$  (Alfa Aesar, 99.95%) were used. The stoichiometric amounts of raw materials were ground in an agate mortar with acetone as a grinding media. The powder blends were transferred into corundum crucibles and calcined at  $1300^\circ\text{C}$  for 6 h. The chromium concentration was varied from 0 to 15%.

The phase purity of the synthesized materials was examined by measurement of X-ray diffraction patterns on a Rigaku MiniFlex II diffractometer. As a radiation source a copper X-ray tube with  $\text{Cu K}\alpha$  radiation ( $\lambda = 1.54 \text{ \AA}$ ) was used. The samples were examined in the region of  $2\theta$  between  $10^\circ$  and  $80^\circ$  with a scanning rate  $10^\circ$  per min.

Excitation and emission spectra were recorded on an Edinburgh Instruments FSL 920 spectrometer equipped with a 450 W Xe arc lamp, mirror optics for powder samples and a cooled ( $-20^\circ\text{C}$ ) single-photon counting photomultiplier (PMT) from Hamamatsu (R2658P), which is sensitive up to 1010 nm. The correction file for the emission spectra was obtained from calibration with a tungsten incandescent lamp certified by NPL (National Physics Laboratory, UK). The decay curves were measured using the same fluorescence spectrometer (Edinburgh Instruments FLS 920). The samples were excited with a Xe- $\mu\text{s}$ -flash lamp.

Diffuse reflection spectra in the 250–800 nm spectral range were recorded on an Edinburgh Instruments FS900 spectrometer equipped with a 450 W Xe arc lamp and a cooled single-photon counting photomultiplier (Hamamatsu R928).  $\text{BaSO}_4$  (Sigma-Aldrich, 99.99%) was used as a reflectance standard. Reflectance spectra in the 120–340 nm spectral range were recorded using an Edinburgh Instruments FLS 920 fluorescence spectrometer equipped with a deuterium lamp DS-775 and a photomultiplier R928 from Hamamatsu. To obtain reflection spectra of the samples excitation scans of powder samples and  $\text{BaMgAl}_{10}\text{O}_{17}:\text{Eu}^{2+}$  (BAM:Eu) were measured in an integration sphere coated with BAM:Eu phosphor. The VUV photons reflected by the sample are completely absorbed by the coated integrating sphere, which in turn emits blue light with a peak wavelength of 450 nm. The VUV/UV reflection spectrum of the sample is obtained by a simple division (excitation spectrum of the sample/excitation spectrum of the BAM:Eu $^{2+}$  powder).

For recording excitation and emission spectra at 3 K a He-cryostat “Optistat AC-V 12” from Oxford Instruments was introduced in the above described Edinburgh Instruments FSL 920 spectrometer. Thermal quenching (TQ) curves were recorded in a cryostat “MicrostatN” from Oxford Instruments. Measurements were carried out from 77 to 500 K in 50 K steps.

## 3. Results and discussion

### 3.1. $\text{Sr}_8\text{MgLa}(\text{PO}_4)_7$ crystal structure

$\text{Sr}_8\text{MgLa}(\text{PO}_4)_7$  ortho-phosphate crystallizes in the Whitlockite type structure corresponding to  $\text{Sr}_9\text{In}(\text{PO}_4)_7$ , which belongs to the monoclinic crystal system with the space group  $\text{I}2/a$  [11]. In the SMLP structure, five different  $\text{Sr}^{2+}$  sites may be distinguished, which are eight-, nine-, and ten-coordinated, whereas  $\text{Mg}^{2+}$  and  $\text{La}^{3+}$  ions occupy octahedral sites.

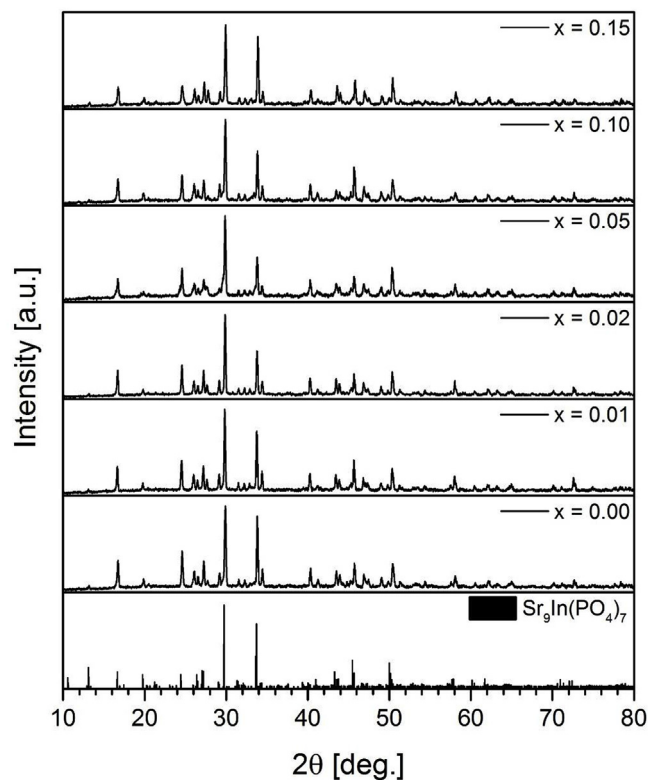


Fig. 1. XRD patterns of  $\mu\text{m}$ -scale powders of undoped  $\text{Sr}_8\text{MgLa}(\text{PO}_4)_7$ ,  $\text{Sr}_8(\text{Mg}_{1-x}\text{Cr}_x)\text{La}(\text{PO}_4)_7$  ( $x = 0.01, 0.02, 0.05, 0.10, 0.15$ ), and ICDD reference data of  $\text{Sr}_9\text{In}(\text{PO}_4)_7$ .

In SMLP, we predict a chromium substitution mainly on  $\text{Mg}^{2+}$  sites due to the large crystal field stabilization energy of  $\text{Cr}^{3+}$  ions on octahedral sites and similarity of the crystal ionic radii of  $\text{Cr}^{3+}$  (75.5 p.m., CN = 6) and  $\text{Mg}^{2+}$  (86.0 p.m., CN = 6) ions. It is unlikely that  $\text{Cr}^{3+}$  ions replace  $\text{La}^{3+}$  (117.2 p.m., CN = 6) or  $\text{Sr}^{2+}$  ions (140 p.m., CN = 8) due to the large difference in ionic radii [13].

Since  $\text{Cr}^{3+}$  and  $\text{Mg}^{2+}$  ions have a different formal charge, substitution of  $\text{Cr}^{3+}$  ion for  $\text{Mg}^{2+}$  ion will lead to charge imbalance. The synthesis of the powders did not involve any univalent ions for balancing the charge difference. Thus, the excess of chromium positive charge requires charge compensation, e.g., by magnesium vacancies. For every two  $\text{Cr}^{3+}$  ions entering the crystal structure, there is one vacant  $\text{Mg}^{2+}$  site [14].

### 3.2. Phase formation – XRD patterns

Crystal structure and phase purity of undoped  $\text{Sr}_8\text{MgLa}(\text{PO}_4)_7$  and  $\text{Sr}_8(\text{Mg}_{1-x}\text{Cr}_x)\text{La}(\text{PO}_4)_7$  ( $x = 0.01–0.15$ ) were examined by recording X-ray diffraction pattern that are plotted in Fig. 1. The position of diffraction patterns and their relative intensities are in good agreement with the reference data ICDD 04-009-5452 of  $\text{Sr}_9\text{In}(\text{PO}_4)_7$  [15].

The samples are single phase even at the higher doping levels of chromium. The increasing  $\text{Cr}^{3+}$  concentration in SMLP does not cause any shift of the X-ray diffraction patterns nor any broadening of the peaks. These findings indicate that there is no significant change in the lattice parameters and structural order due to the high  $\text{Cr}^{3+}$  concentration.

A higher concentration of  $\text{Cr}^{3+}$  than 15% in SMLP leads to the formation of impurity phases. The XRD patterns of highly  $\text{Cr}^{3+}$  doped samples (not shown here) showed a presence of some moieties of  $\text{Sr}_4[\text{CrO}_4][\text{PO}_4]_2$  and unreacted  $\text{Cr}_2\text{O}_3$ . As these samples are not single phase, the optical properties of SMLP: $x\text{Cr}^{3+}$  ( $x > 0.15$ ) have not been investigated.

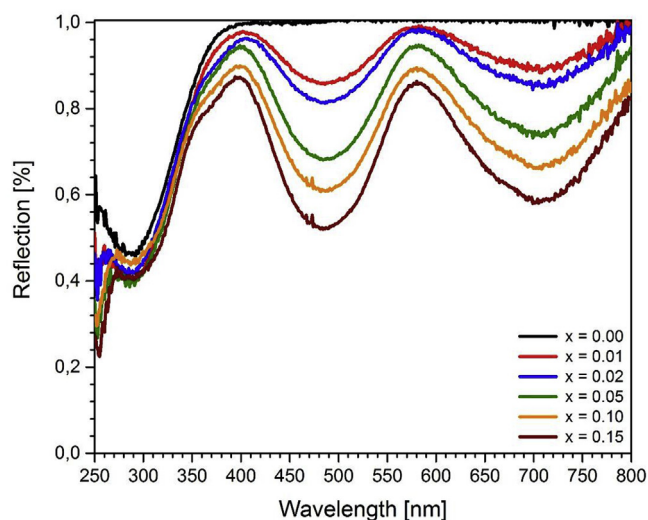


Fig. 2. Reflection spectra of undoped  $\text{Sr}_8\text{MgLa}(\text{PO}_4)_7$  and  $\text{Sr}_8(\text{Mg}_{1-x}\text{Cr}_x)\text{La}(\text{PO}_4)_7$  ( $x = 0.01, 0.02, 0.05, 0.10, 0.15$ ).

### 3.3. Optical properties at room temperature

Fig. 2 displays diffuse reflection spectra for a sample of undoped  $\text{Sr}_8\text{MgLa}(\text{PO}_4)_7$  and for  $\text{Sr}_8(\text{Mg}_{1-x}\text{Cr}_x)\text{La}(\text{PO}_4)_7$  ( $x = 0.01, 0.02, 0.05, 0.10, 0.15$ ) samples. The undoped SMLP sample exhibits high reflectance in the visible spectral range indicating a high brightness of the prepared powder. The reflection spectrum of SMLP:1%Cr shows two broad absorption bands with maxima at around 485 nm and 700 nm, which can be assigned to the spin-allowed  $^4A_2 \rightarrow ^4T_1$  and  $^4A_2 \rightarrow ^4T_2$  transitions of  $\text{Cr}^{3+}$  ion, respectively.

Additionally, at around 288 nm, there is a broad absorption band, which also appears in the undoped SMLP. Similar absorption bands below 350 nm were observed by Huang et al. in  $\text{Eu}^{2+}$  activated  $\text{Sr}_8\text{MgLa}(\text{PO}_4)_7$  and  $\text{Sr}_8\text{ZnSc}(\text{PO}_4)_7$  [11,16]. They assigned these bands to the host absorption bands and have estimated the energy of the band gaps to 4.15 eV and 4.34 eV, respectively. Nonetheless, as determined band gaps energies for ortho-phosphates seem to be quite low. Therefore, it is worthwhile to compare these values with results reported for other ortho-phosphates. For instance, the absorption edges of  $\text{YPO}_4$ ,  $\text{LaPO}_4$  and  $\text{Sr}_3(\text{PO}_4)_2$  (the same energy absorption), and  $\text{ScPO}_4$  were observed at 152 nm, 157 nm, and 168 nm, respectively [17–19]. This indicates that the host lattice absorption edges of some ortho-phosphates occur in the vacuum ultraviolet (VUV) and their band gap lies in the 7–8 eV range.

To examine the host lattice absorption edge in SMLP lattice, reflection spectra of undoped SMLP and Cr-doped SMLP samples were recorded between 120 and 340 nm and are depicted in Fig. 3. The VUV/UV reflection spectra confirm that the host absorption edge of the SMLP matrix occurs at much higher energy than  $\sim 4$  eV, viz. at 7.9 eV (156 nm). The doping of the  $\text{Sr}_8\text{MgLa}(\text{PO}_4)_7$  with  $\text{Cr}^{3+}$  ions results in an additional absorption band extending from 180 to 280 nm. The presence of these bands in SMLP:Cr samples can be due to the charge transfer from  $\text{O}^{2-}$  ligands to  $\text{Cr}^{3+}$  ions. Similar absorption bands in the VUV region were observed in  $\text{Al}_2\text{O}_3:\text{Cr}^{3+}$  and has been assigned to  $\text{O}^{2-} - \text{Cr}^{3+}$  charge transfer bands [20]. The VUV/UV measurements have clearly shown, that the unexpected absorption band with maximum at  $\sim 288$  nm cannot be ascribed to the host absorption edge of  $\text{Sr}_8\text{MgLa}(\text{PO}_4)_7$ . The presence of this band is not clear and further study is required to determine its origin. Possibly, the band is related to UV-absorbing defects (color centers).

Excitation and emission spectra of  $\text{Sr}_8\text{MgLa}(\text{PO}_4)_7:1\%\text{Cr}$  are depicted in Fig. 4. The excitation spectrum was measured for a single emission wavelength ( $\lambda_{\text{em}} = 870$  nm) and reveals three excitation

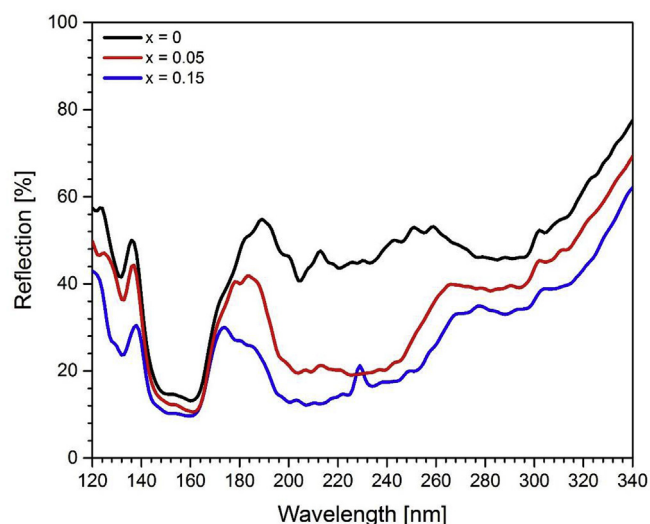


Fig. 3. VUV Reflection spectra of undoped  $\text{Sr}_8\text{MgLa}(\text{PO}_4)_7$  and  $\text{Sr}_8(\text{Mg}_{1-x}\text{Cr}_x)\text{La}(\text{PO}_4)_7$  ( $x = 0.05, 0.15$ ).

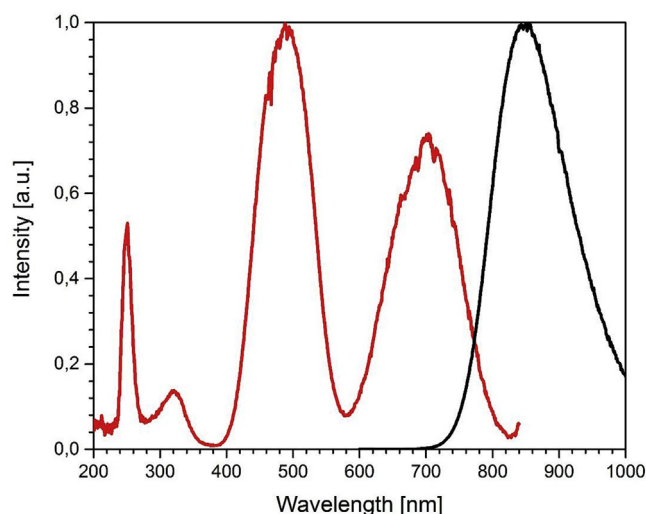


Fig. 4. Excitation (red line,  $\lambda_{\text{em}} = 870$  nm) and emission (black line,  $\lambda_{\text{ex}} = 490$  nm) spectra of  $\text{Sr}_8\text{MgLa}(\text{PO}_4)_7:1\%\text{Cr}$  recorded at room temperature. (For interpretation of the references to color in this figure legend, the reader is referred to the Web version of this article.)

Table 1

Crystal field strength, Racah parameters and  $\beta$ -covalency of  $\text{Sr}_8\text{MgLa}(\text{PO}_4)_7:1\%\text{Cr}^{3+}$  determined from the maximum of the  $^4A_2 \rightarrow ^4T_1$  and  $^4A_2 \rightarrow ^4T_2$  absorption peaks and maxima of emission and excitation bands of  $\text{Sr}_8\text{MgLa}(\text{PO}_4)_7:1\%\text{Cr}^{3+}$ .

Transition/Parameter	$\text{Sr}_8\text{MgLa}(\text{PO}_4)_7:1\%\text{Cr}^{3+}$
$\text{O}^{2-} - \text{Cr}^{3+}$ CT	250 nm/40000 $\text{cm}^{-1}$
$E(^4A_2 \rightarrow ^4T_1(^4P))$	320 nm/31250 $\text{cm}^{-1}$
$E(^4A_2 \rightarrow ^4T_1(^4F))$	488 nm/20492 $\text{cm}^{-1}$
$E(^4A_2 \rightarrow ^4T_2(^4F))$	704 nm/14205 $\text{cm}^{-1}$
$E(^4T_2(^4F) \rightarrow ^4A_2)$	848 nm/11792 $\text{cm}^{-1}$
$D_q$	1421 $\text{cm}^{-1}$
$B$	686 $\text{cm}^{-1}$
$10 Dq/B$	20.7
$\beta = B/B_0$	0.75

bands typical of  $\text{Cr}^{3+}$  ion located in the UV, cyan and deep red spectral range (Table 1). The excitation bands are attributed to the spin-allowed  $^4A_2 \rightarrow ^4T_1(^4P)$ ,  $^4A_2 \rightarrow ^4T_1(^4F)$  and  $^4A_2 \rightarrow ^4T_2(^4F)$  transitions of  $\text{Cr}^{3+}$ ,



respectively. Besides 3d-3d excitation bands, a fourth band in the UV range appears ( $\lambda_{\text{max}} \sim 250$  nm) and it is assigned to the  $\text{O}^{2-} - \text{Cr}^{3+}$  charge transfer band. The emission spectrum of  $\text{Sr}_8\text{MgLa}(\text{PO}_4)_7:1\%\text{Cr}$  was recorded upon excitation at 490 nm and displays a broad band NIR emission corresponding to the spin-allowed  ${}^4\text{T}_2 \rightarrow {}^4\text{A}_2$  transition of  $\text{Cr}^{3+}$  ion. The emission band extends from 700 to 1000 nm (or even longer wavelengths) and a full width at half maximum (FWHM) is around 141 nm ( $1917\text{ cm}^{-1}$ ). The emission due to the spin-forbidden  ${}^2\text{E} \rightarrow {}^4\text{A}_2$  transition (also known as R-line) has not been detected and this indicates that  $\text{Cr}^{3+}$  ion occupies weak crystallographic sites in SMLP.

As the  $\text{Cr}^{3+}$  ion has a  $[\text{Ar}]3\text{d}^3$  electron configuration, the 3d electrons are not shielded by outer shells and the optical properties of trivalent chromium are sensitive to the environment. This gives rise to a strong interaction of  $\text{Cr}^{3+}$  with the crystal field and lattice vibrations in the crystals. The impact of the host lattice on the  $\text{Cr}^{3+}$  photoluminescence can be expressed by spectroscopic parameters such as the crystal field splitting ( $10Dq$ ),  $B$  Racah parameter and  $\beta$ -covalency ( $B/B_0$ ). The spectroscopic parameters were calculated from the energy maxima of the  ${}^4\text{A}_2 \rightarrow {}^4\text{T}_1$  ( ${}^4\text{P}$ ),  ${}^4\text{A}_2 \rightarrow {}^4\text{T}_1$  ( ${}^4\text{F}$ ) and  ${}^4\text{A}_2 \rightarrow {}^4\text{T}_2$  ( ${}^4\text{F}$ ) absorption bands of SMLP:1%Cr and are collected in Table 1.

The crystal field splitting parameter  $Dq$  and  $B$  Racah parameter for SMLP:1%Cr are  $1421\text{ cm}^{-1}$  and  $686\text{ cm}^{-1}$ , respectively. By comparing the values of these parameters with parameters for  $\text{Cr}^{3+}$  occupying strong crystal field sites, e.g., in  $\text{Al}_2\text{O}_3:1\%\text{Cr}^{3+}$  ( $Dq = 1799\text{ cm}^{-1}$ ,  $B = 619\text{ cm}^{-1}$ ),  $\text{MgAl}_2\text{O}_4:1\%\text{Cr}^{3+}$  ( $Dq = 1715\text{ cm}^{-1}$ ,  $B = 620\text{ cm}^{-1}$ ), and  $\text{LaAlO}_3:1\%\text{Cr}^{3+}$  ( $Dq = 1635\text{ cm}^{-1}$ ,  $B = 513\text{ cm}^{-1}$ ) [21], we can conclude that the  $\text{Sr}_8\text{MgLa}(\text{PO}_4)_7:1\%\text{Cr}^{3+}$  phosphor belongs to weak crystal field materials like  $\text{SrSc}_2\text{O}_4:\text{Cr}^{3+}$  ( $Dq = 1471\text{ cm}^{-1}$ ,  $B = 700\text{ cm}^{-1}$ ) [22] or  $\text{La}_3\text{Sc}_2\text{Ga}_3\text{O}_{12}:\text{Cr}^{3+}$  ( $Dq = 1458\text{ cm}^{-1}$ ,  $B = 642\text{ cm}^{-1}$ ) [23]. The value of the  $\beta$ -covalency for SMLP:1%Cr is rather high for  $\text{Cr}^{3+}$  in an oxide and amounts to 0.75. This indicates on a small spatial expansion of the  $d$  electron wavefunctions in the crystals (weak nephelauxetic effect). The value of  $10Dq/B$  for SMLP:1%Cr is 20.7 and according to the Tanabe-Sugano diagram for  $d^3$  electronic configuration in octahedral symmetry, the  ${}^4\text{T}_2$  level lies below the  ${}^2\text{E}$  level [24]. The spectroscopic parameters for SMLP:1%Cr denote a weak crystal field acting on Cr ions in SMLP lattice. This explains the absence of the R-line emission and the observation of a dominant  ${}^4\text{T}_2$  broad band emission.

In order to investigate the influence of the  $\text{Cr}^{3+}$  concentration on the photoluminescence properties of  $\text{Sr}_8\text{MgLa}(\text{PO}_4)_7:x\text{Cr}^{3+}$  a series of powders was prepared with Cr concentration ranging from 1 to 15%. A gradual increase in  $\text{Cr}^{3+}$  concentration in SMLP provides a stronger absorption in the visible spectral range (Fig. 2) and a higher intensity of  ${}^4\text{A}_2 \rightarrow {}^4\text{T}_2$  and  ${}^4\text{A}_2 \rightarrow {}^4\text{T}_1$  excitation bands (Fig. 5). The position of d-d absorption and excitation bands does not change with increasing Cr concentration and indicate a negligible influence of the chromium content on the crystal field splitting of 3d orbitals. The intensity of broad band emission of  $\text{Cr}^{3+}$  in SMLP (Fig. 6) increases with increasing  $\text{Cr}^{3+}$  concentration and reaches maximum at 15%. An even further increase of  $\text{Cr}^{3+}$  in SMLP caused a decrease of the photoluminescence intensity that can be explained by the presence of the impurities and concentration quenching.

The increasing Cr concentration in SMLP gives rise to a shift of the emission maxima to longer wavelengths (lower energy) (Fig. 6). If the concentration of  $\text{Cr}^{3+}$  ions is increased from 1 to 15%, the emission spectra are red shifted by  $\sim 10$  nm. Similar red shift upon increasing concentration of the activator was observed in  $\text{Al}_2\text{O}_3:\text{Cr}^{3+}$  and  $\text{Zn}_2\text{SiO}_4:\text{Mn}^{2+}$  [25–27] and was attributed to exchange interactions between  $\text{Cr}^{3+}$  and  $\text{Mn}^{2+}$  ions, respectively. The probability of pair formation increases as the square of the  $\text{Cr}^{3+}$  concentration and a red shift of the  ${}^4\text{T}_2$  chromium emission in SMLP can occur ongoing from single  $\text{Cr}^{3+}$  ions to  $\text{Cr}^{3+}$  pairs due to lattice distortions by neighboring  $\text{Cr}^{3+}$  ions [28,29].

The emission from single ions,  $\text{Cr}^{3+}$  pairs, and  $\text{Cr}^{3+}$  clusters can be spectrally resolved in materials exhibiting strong crystal field sites. For

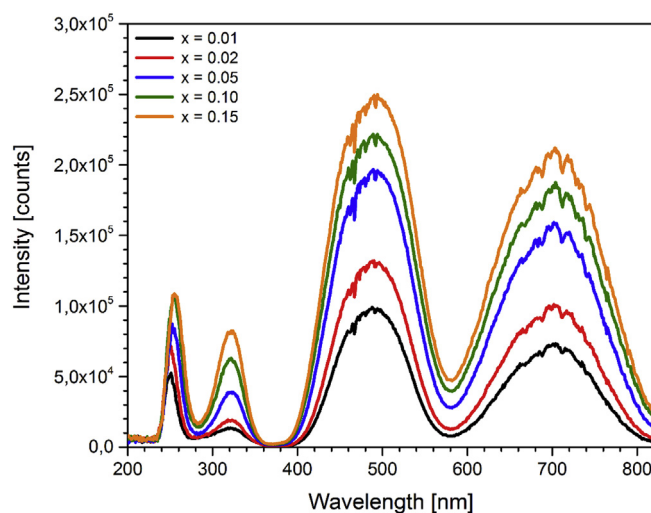


Fig. 5. Excitation of  $\text{Sr}_8\text{MgLa}(\text{PO}_4)_7$  doped with different  $\text{Cr}^{3+}$  concentration ( $x = 0.01, 0.02, 0.05, 0.10, 0.15$ ) recorded for 870 nm emission at room temperature.

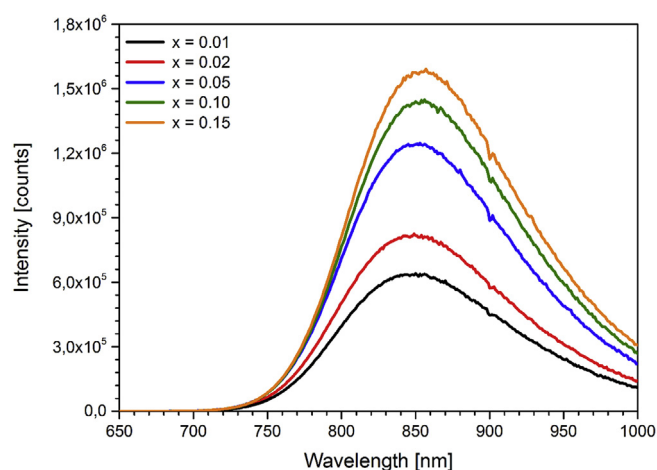


Fig. 6. Emission spectra of  $\text{Sr}_8\text{MgLa}(\text{PO}_4)_7$  doped with different  $\text{Cr}^{3+}$  concentration ( $x = 0.01, 0.02, 0.05, 0.10, 0.15$ ) recorded upon 490 nm excitation at room temperature.

instance, in  $\text{Al}_2\text{O}_3:\text{Cr}^{3+}$  the  ${}^2\text{E} \rightarrow {}^4\text{A}_2$  emission of  $\text{Cr}^{3+}$  isolated ions at low temperature is observed as a narrow line peaking at 693.1 nm, whereas the  $\text{Cr}^{3+}$  pairs and  $\text{Cr}^{3+}$  cluster emission appears at longer wavelengths as sharp lines at  $\sim 700$  nm and broad bands extending from  $\sim 740$  nm to 840 nm, respectively [30–32]. In the case of  $\text{Cr}^{3+}$  doped  $\text{Sr}_8\text{MgLa}(\text{PO}_4)_7$ , the  ${}^4\text{T}_2 \rightarrow {}^4\text{A}_2$  emission band of single  $\text{Cr}^{3+}$  exhibits strong electron-phonon coupling and thus a strong overlap with  $\text{Cr}^{3+}$  pairs emission, so that the presence of  $\text{Cr}^{3+}$  pairs cannot be spectrally resolved even at low temperature.

For further investigation of the  $\text{Cr}^{3+}$  pair formation and concentration quenching, measurements of decay curves for  $\text{Sr}_8(\text{Mg}_{1-x}\text{Cr}_x)\text{La}(\text{PO}_4)_7$  ( $x = 0.01, 0.02, 0.05, 0.10, 0.15$ ) at room temperature were performed. Luminescence decay times were monitored at 800 nm upon pulsed excitation at 490 nm and are depicted in Fig. 7. The decay curves for a low  $\text{Cr}^{3+}$  concentration ( $x = 0.01$ – $0.05$ ) are single exponential, whereas at higher concentrations, the decay curves become slightly non-exponential. The lifetimes were obtained from the decay curves fitting to a single exponential function.

The inset in Fig. 7 displays the decay times of  $\text{Cr}^{3+}$  emission as a function of the concentration. As can be observed, the emission lifetime gradually decreases upon increasing activator concentration and changes from 105  $\mu\text{s}$  to 70  $\mu\text{s}$  for samples with 1% and 15% of

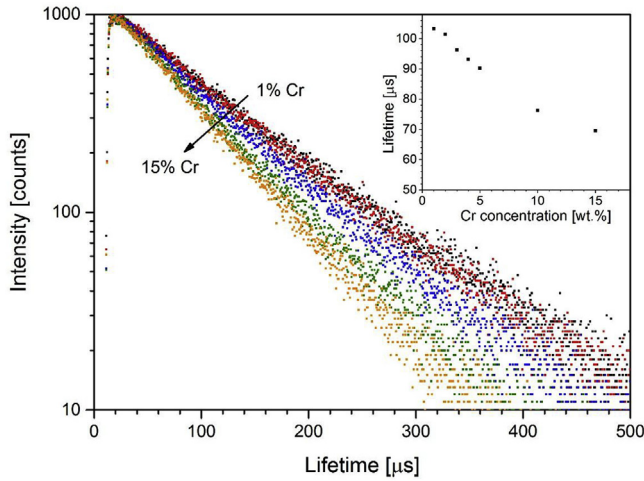


Fig. 7. Photoluminescence decay curves of  $\text{Sr}_8(\text{Mg}_{1-x}\text{Cr}_x)\text{La}(\text{PO}_4)_7$  ( $x = 0.01, 0.02, 0.05, 0.10, 0.15$ ) monitored at 800 nm upon excitation at 490 nm at room temperature.

$\text{Cr}^{3+}$ , respectively. The shortening of the  $\text{Cr}^{3+}$  emission lifetime could be an evidence that concentration quenching sets in. Alternatively, the decrease of the lifetime can be the result of local symmetry distortions in  $\text{Cr}^{3+}$  pairs which partly lifts the parity selection rule for  $\text{Cr}^{3+}$  ions in the centrosymmetric lattice sites. Therefore, the slightly non-exponential decay behavior at higher Cr concentrations in SMLP can be due to the simultaneous emission from single  $\text{Cr}^{3+}$  ions and emission from  $\text{Cr}^{3+}$  pairs which is characterized by a shorter lifetime [30].

### 3.4. Optical properties at liquid helium temperature

As the thermal broadening and interactions between neighboring  $\text{Cr}^{3+}$  ions at room temperature have a significant impact on the luminescence properties of  $\text{Cr}^{3+}$  in  $\text{Sr}_8\text{MgLa}(\text{PO}_4)_7$ , low temperature measurements for the sample doped with 1% of  $\text{Cr}^{3+}$  (expected single  $\text{Cr}^{3+}$  ions) were done. Measurements at liquid helium temperature reveal spectral details that are not apparent at a higher temperature and allow an accurate determination of the Stokes shift and Huang-Rhys parameter  $S$ , whereas temperature dependent emission spectra and decay time measurements provide insight in thermal quenching of the  $\text{Cr}^{3+}$  emission.

Fig. 8 displays emission spectrum of SMLP:1%Cr measured at 3 K upon excitation at 490 nm. The broad band NIR emission is attributed to the  ${}^4\text{T}_2 \rightarrow {}^4\text{A}_2$  transition. The absence of the  ${}^2\text{E}$  emission in the spectrum confirms that the  ${}^4\text{T}_2$  state is the lowest excited state for  $\text{Cr}^{3+}$  in the  $\text{Sr}_8\text{MgLa}(\text{PO}_4)_7$  ortho-phosphate. The low temperature  ${}^4\text{T}_2$  emission band of  $\text{Cr}^{3+}$  (FWHM =  $1428 \text{ cm}^{-1}$ ,  $\lambda_{\text{max}} = 830 \text{ nm}$ ) is narrower and blue shifted by  $\sim 20 \text{ nm}$  in comparison to the emission spectrum measured at RT (Table 2). The fine structure of the broad emission spectrum reveals a sharp and very weak line at around  $748.5 \text{ nm}$  ( $13360 \text{ cm}^{-1}$ ). This narrow peak is assigned to the  ${}^4\text{T}_2 \rightarrow {}^4\text{A}_2$  zero-phonon line (ZPL) transition.

Photoluminescence spectra recorded at 3 K allow more precise determination of the values for the Stokes shift ( $\Delta E_{\text{ss}}$ ) and Huang-Rhys parameter  $S$  (Table 2) due to a negligible thermal broadening at low temperature. The Stokes shift was estimated from the energy difference between the excitation and emission maxima ( $\Delta E_{\text{ss}} = E({}^4\text{A}_2 \rightarrow {}^4\text{T}_2) - E({}^4\text{T}_2 \rightarrow {}^4\text{A}_2)$ ) and amounts to  $\sim 2487 \text{ cm}^{-1}$ . The Huang-Rhys parameter  $S$  was evaluated from the relative position of the zero-phonon line  $I_{\text{ZPL}} = I_0 \cdot \exp(-S)$  and has a value of  $\sim 8$  [33]. The value for the  $S$  parameter is consistent with the observed Stokes shift and a vibrational energy of  $\sim 160 \text{ cm}^{-1}$  ( $\Delta E_{\text{ss}} = 2S\hbar\omega = 2480 \text{ cm}^{-1}$ ).

### 3.5. Temperature dependent $\text{Cr}^{3+}$ PL in $\text{Sr}_8\text{MgLa}(\text{PO}_4)_7$

Thermal quenching of the  $\text{Cr}^{3+}$  emission in  $\text{Sr}_8\text{MgLa}(\text{PO}_4)_7$  was investigated by temperature dependent emission spectra and temperature dependent lifetime measurements recorded between 77 and 500 K.

Fig. 9 shows temperature dependent emission spectra of SMLP:1% $\text{Cr}^{3+}$ . The position of the emission bands shows strong temperature dependence. In addition to thermal broadening, the emission spectrum at 400 K is red shifted by about  $420 \text{ cm}^{-1}$  ( $\sim 30 \text{ nm}$ ) compared to the spectrum recorded at 77 K. At a higher temperature than 400 K the emission bands are significant quenched, and determination of the emission maxima is inaccurate. The red shift upon heating is commonly observed for emission from 3d transition metal ions at higher temperatures and can be explained by lattice expansion causing the crystal field splitting to decrease.

In Fig. 10 the normalized integral emission intensity of the  $\text{Cr}^{3+}$  broad band emission in  $\text{Sr}_8(\text{Mg}_{1-x}\text{Cr}_x)\text{La}(\text{PO}_4)_7$  ( $x = 0.01, 0.05, 0.15$ ) as a function of temperature between 77 and 500 K are displayed. In the low temperature regime (up to 200 K), the emission intensity of 1% Cr and 5% Cr in SMLP is constant. Thermal quenching for these samples starts at around 250 K, whereas thermal quenching in SMLP:15%Cr sets in already at 200 K.

In order to determine the quenching temperature ( $T_{1/2}$  is the temperature where the emission intensity reaches 50% of its maximum) a Fermi-Dirac fit was used:

$$I(T) = \frac{I_0}{1 + A \cdot e^{\frac{-\Delta E_{\text{act}}}{kT}}} \quad (1)$$

where  $I(T)$  is the PL intensity at a certain temperature,  $I_0$  is the PL intensity at 0 K,  $A$  is the frequency factor for thermal quenching,  $\Delta E_{\text{act}}$  is the activation energy for thermal quenching,  $k$  is the Boltzmann constant, and  $T$  is the temperature. Parameters  $I_0$  and  $A$  were obtained from the fitting function and are collected in Table 3. The quenching temperatures were calculated based on the following formula:

$$T_{1/2} = -\frac{\Delta E_{\text{act}}}{k \cdot \ln\left(\frac{1}{A}\right)} \quad (2)$$

The obtained  $T_{1/2}$  values for the broad band  $\text{Cr}^{3+}$  emission in SMLP:1%Cr, SMLP:5%Cr, and SMLP:15%Cr are 317 K, 305 K, and 289 K, respectively (Table 3). This indicates that the samples doped with low activator concentration exhibit better thermal stability of the  ${}^4\text{T}_2$  emission of  $\text{Cr}^{3+}$ . This is also reflected by a larger activation energy for thermal quenching in SMLP:1%Cr ( $\Delta E_{\text{act}} = 0.29 \text{ eV}$ ) than in SMLP:15%Cr ( $\Delta E_{\text{act}} = 0.23 \text{ eV}$ ). The slightly lower  $T_{1/2}$  values for highly doped  $\text{Sr}_8\text{MgLa}(\text{PO}_4)_7$  lattice can be explained by a higher probability of non-radiative processes originating from thermally activated concentration quenching.

It is worthwhile to compare the quenching behavior of the  ${}^4\text{T}_2 \rightarrow {}^4\text{A}_2$  emission of  $\text{Cr}^{3+}$  in SMLP with other broad band NIR  $\text{Cr}^{3+}$  phosphors. Table 4 shows spectroscopic parameters for  $\text{Cr}^{3+}$  in  $\text{CaSc}_2\text{O}_4$  [22],  $\text{Sr}_8\text{MgLa}(\text{PO}_4)_7$ , and  $\text{La}_3\text{Sc}_2\text{Ga}_3\text{O}_{12}$  (LaSGG) [23]. In these materials  $\text{Cr}^{3+}$  ions occupy weak crystal field sites ( $E({}^4\text{T}_2) < E({}^2\text{E})$ ) which is in line with a low crystal field splitting parameter ( $Dq < 1500 \text{ cm}^{-1}$ ). The large spectral bandwidth (FWHM  $> 140 \text{ nm}$ ) and corresponding high Huang-Rhys parameter ( $S > 5$ ) indicate a strong electron-phonon coupling for the  ${}^4\text{T}_2 \rightarrow {}^4\text{A}_2$  transition, which has a significant impact on thermal quenching of Cr PL. The quenching of the  ${}^4\text{T}_2$  emission of  $\text{Cr}^{3+}$  is ascribed to thermally activated cross-over from the  ${}^4\text{T}_2$  excited state to the  ${}^4\text{A}_2$  ground as can be depicted in a configurational coordinate diagram. The quenching temperature strongly depends on the relaxation in the excited state (stronger relaxation, i.e. larger Stokes shift and Huang-Rhys parameter  $S$ , results in lower  $T_{1/2}$ ). The large Stokes shift ( $\Delta E_{\text{ss}} = 3042 \text{ cm}^{-1}$ ) for  $\text{CaSc}_2\text{O}_4:\text{Cr}$  explains why thermal quenching of  $\text{Cr}^{3+}$  luminescence starts already at low temperature, i.e. at 77 K and results in a very low quenching temperature

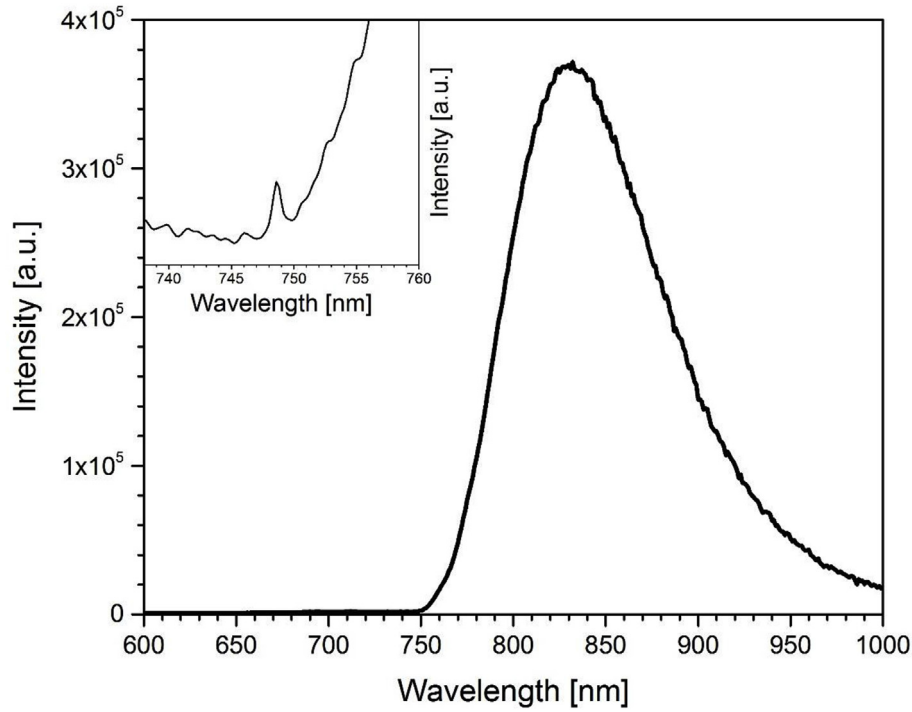


Fig. 8. Emission spectrum of  $\text{Sr}_8\text{MgLa}(\text{PO}_4)_7:1\%\text{Cr}$  measured upon 490 nm excitation at 3 K. The inset displays the  $^4\text{T}_2 \rightarrow ^4\text{A}_2$  zero-phonon line.

Table 2

Spectroscopic parameters for  $\text{Sr}_8\text{MgLa}(\text{PO}_4)_7:1\%\text{Cr}^{3+}$  determined at 3 K and from temperature dependent photoluminescence measurements in the 77–500 K temperature range.

Parameter	$\text{Sr}_8\text{MgLa}(\text{PO}_4)_7:1\%\text{Cr}^{3+}$
FWHM (RT)	141 nm/1917 $\text{cm}^{-1}$
FWHM (3 K)	100 nm/1428 $\text{cm}^{-1}$
$\Delta E_{\text{ss}}$ (3 K)	2487 $\text{cm}^{-1}$
ZPL ( $^4\text{T}_2$ )	748.5 nm/13360 $\text{cm}^{-1}$
$T_{1/2}$	320 K
$E_{\text{act}}$	0.29 eV
$S$	7.9
$\hbar\omega$	157 $\text{cm}^{-1}$

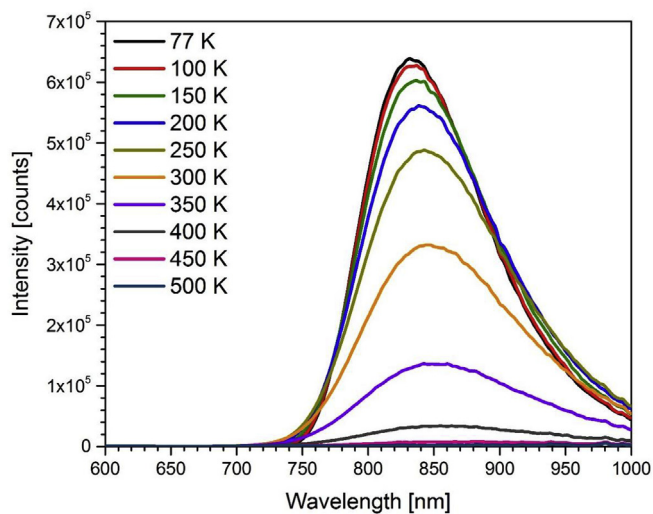


Fig. 9. Temperature dependent emission spectra of  $\text{Sr}_8\text{MgLa}(\text{PO}_4)_7:1\%\text{Cr}^{3+}$  recorded upon excitation at 490 nm in the temperature range from 77 to 500 K.

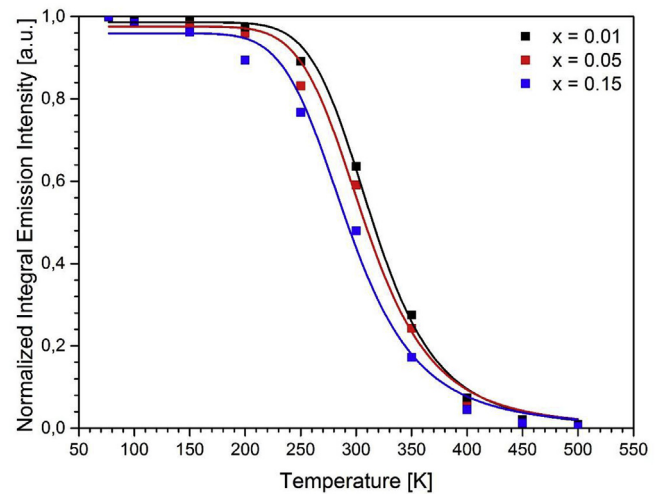


Fig. 10. Normalized integral emission intensity of the  $\text{Cr}^{3+}$  broad band emission in  $\text{Sr}_8(\text{Mg}_{1-x}\text{Cr}_x)\text{La}(\text{PO}_4)_7$  ( $x = 0.01, 0.05, 0.15$ ) measured upon 490 nm excitation between 77 and 500 K.

Table 3

Parameters obtained from a Fermi-Dirac fit of experimental data.

Parameter	SMLP:1%Cr	SMLP:5% Cr	SMLP:15%Cr
$I_0$	0.986	0.976	0.960
$A$	$4.06 \cdot 10^4$	$1.96 \cdot 10^4$	$1.01 \cdot 10^4$
$T_{1/2}$	317 K	305 K	289 K
$\Delta E_{\text{act}}$	0.29 eV	0.26 eV	0.23 eV

( $T_{1/2} < 240$  K). The Stokes shift for the  $\text{Cr}^{3+}$  emission in SMLP:Cr and LaSGG:Cr ( $\Delta E_{\text{ss}} < 2500 \text{ cm}^{-1}$ ) is much smaller than for  $\text{CaSc}_2\text{O}_4:\text{Cr}$  and give rise to a higher  $T_{1/2}$ . However, the difference in  $\Delta E_{\text{ss}}$  for these two Cr-phosphors is small ( $\sim 100 \text{ cm}^{-1}$ ) and another factor contributing to low quenching temperature has to be considered to explain the difference in  $T_{1/2}$ . According to work of Blasse, for the same Stokes



**Table 4**

Spectroscopic parameters for  $\text{Cr}^{3+}$  in different host lattices including crystal field splitting parameter  $Dq$ , emission maximum at RT ( $\lambda_{\text{em}}$ ), spectral bandwidth of emission (FWHM), Stokes shift ( $\Delta E_{\text{ss}}$ ), energy position of the  $^4\text{T}_2$  zero phonon line, and quenching temperature ( $T_{1/2}$ ).

Host composition	$Dq$	$\lambda_{\text{em}}$	FWHM	Stokes shift	ZPL $^4\text{T}_2$	$T_{1/2}$
$\text{CaSc}_2\text{O}_4$ [22]	$1471 \text{ cm}^{-1}$	820 nm	164 nm	$3042 \text{ cm}^{-1}$	$13550 \text{ cm}^{-1}$	< 240 K
$\text{Sr}_8\text{MgLa}(\text{PO}_4)_7$	$1421 \text{ cm}^{-1}$	848 nm	141 nm	$2487 \text{ cm}^{-1}$	$13360 \text{ cm}^{-1}$	317 K
$\text{La}_3\text{Sc}_2\text{Ga}_3\text{O}_{12}$ [23]	$1458 \text{ cm}^{-1}$	818 nm	145 nm	$2392 \text{ cm}^{-1}$	$13605 \text{ cm}^{-1}$	450 K

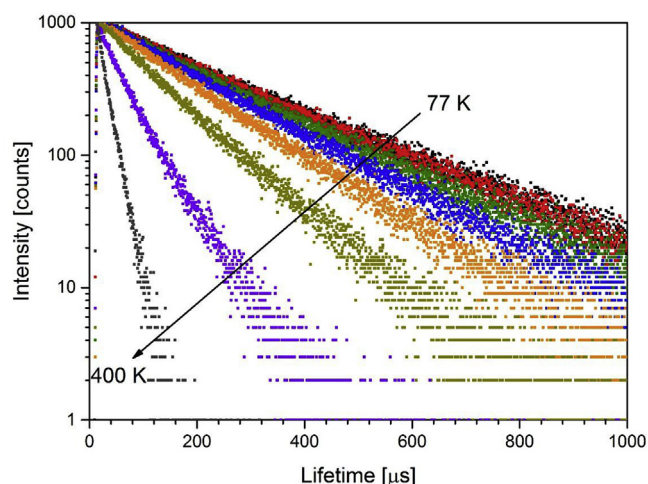


**Fig. 11.** Photoluminescence decay curves of  $\text{Sr}_8\text{MgLa}(\text{PO}_4)_7:1\%\text{Cr}^{3+}$  monitored at 800 nm upon excitation at 490 nm between 77 and 400 K.

shift, a lower energy excited state leads to lower luminescence quenching temperatures. Indeed, the  $Dq$  parameter for SMLP:Cr is lower than for LaSGG:Cr and this causes a shift of the  $^4\text{T}_2$  emission band to lower energy (longer wavelengths). The lower energy of  $^4\text{T}_2$  level in SMLP:Cr can explain the lower  $T_{1/2}$  in comparison to LaSGG:Cr. To realize an efficient broad band NIR emitting phosphor based on  $^4\text{T}_2$  emission from  $\text{Cr}^{3+}$  a small Stokes shift has to be coupled to a relatively high energy emission.

Thermal quenching of  $\text{Cr}^{3+}$  PL in  $\text{Sr}_8\text{MgLa}(\text{PO}_4)_7$  was also investigated by measurements of the luminescence lifetimes of  $\text{Cr}^{3+}$  emission at different temperatures. Fig. 11 shows temperature dependent decay curves of the  $^4\text{T}_2$  emission of  $\text{Cr}^{3+}$  ions in SMLP:1%. Emission was monitored at 800 nm upon pulsed excitation at 490 nm. The decay curves are close to single exponential. The lifetimes were determined from the single exponential fitting of the decay curves and are displayed as a function of temperature in Fig. 12 (red dots).

At low temperatures a  $\mu\text{s}$  decay time ( $\tau = 240 \mu\text{s}$  at 77 K) is observed. Since the energy of the  $^2\text{E}$  level is higher than the energy of the  $^4\text{T}_2$  level ( $\Delta E = -1166 \text{ cm}^{-1}$ ), the doublet state is hardly populated for excited  $\text{Cr}^{3+}$  ions and a negligible impact on the emission lifetime is expected. Generally, the lifetime of the spin-allowed  $^4\text{T}_2 \rightarrow ^4\text{A}_2$  transition of  $\text{Cr}^{3+}$  in low symmetry sites is of the order of a few microseconds, like in  $\text{CaSc}_2\text{O}_4:\text{Cr}$  ( $\tau \sim 25 \mu\text{s}$  at 77 K) [22]. The  $\sim 10$  times longer decay time for SMLP:Cr at low temperature may indicate on the  $\text{Cr}^{3+}$  substitution for the  $\text{Mg}^{2+}$  ions, which are in sites of perfect octahedral symmetry. The same phenomenon was observed in  $\text{Na}_3\text{Ga}_2\text{Li}_3\text{F}_{12}:\text{Cr}$  [34]. In this material  $\text{Cr}^{3+}$  ion substitute for  $\text{Ga}^{3+}$  ions in the inversion site symmetry and this give rise to a long lifetime ( $\tau = 310 \mu\text{s}$ ) of the  $\text{Cr}^{3+}$  emission.

In the case of low-field  $\text{Cr}^{3+}$  materials, it is expected that the photoluminescence intensity and the lifetime of  $\text{Cr}^{3+}$  emission are mainly determined by the radiative and non-radiative processes of the  $^4\text{T}_2 \rightarrow ^4\text{A}_2$  transition. Hence, the temperature dependence of the emission intensity and lifetime of  $\text{Cr}^{3+}$  are expected to be similar, e.g., in the case of  $\text{LiSrAlF}_6:\text{Cr}$  [35]. In the low temperature regime, the lifetimes of

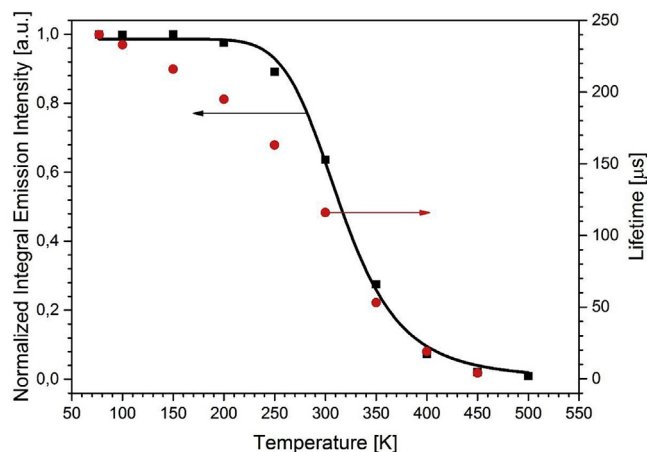


**Fig. 12.** Normalized integral emission intensity (black dots) and decay time of the  $\text{Cr}^{3+}$  broad band emission (red dots,  $\lambda_{\text{em}} = 800 \text{ nm}$ ) in  $\text{Sr}_8\text{MgLa}(\text{PO}_4)_7:1\%\text{Cr}^{3+}$  as a function of temperature. The solid line corresponds to the Fermi-Dirac fit. (For interpretation of the references to color in this figure legend, the reader is referred to the Web version of this article.)

$\text{Cr}^{3+}$  emission in SMLP show a small deviation from the curve displaying the temperature dependence of the emission intensity (Fig. 12). The emission intensity remains constant between 77 and 250 K, whereas the luminescence lifetime decreases with an increase of temperature. A faster initial decrease of the lifetime at low temperature (between 70 and 200 K) can occur due to vibronically induced  $^4\text{T}_2 \rightarrow ^4\text{A}_2$  transitions. For  $\text{Cr}^{3+}$  in inversion site symmetry coupling with odd-parity vibrations can lift the symmetry selection rule. Upon thermal population of these odd-parity vibrations the vibronic transition probability increases and the radiative lifetime decreases. A similar effect in absorption and emission has also been reported for the isoelectronic  $\text{Mn}^{4+}$  ion [36].

#### 4. Conclusions

The photoluminescence of  $\text{Cr}^{3+}$  in an ortho-phosphate with chemical composition  $\text{Sr}_8\text{MgLa}(\text{PO}_4)_7$  was investigated for the first time. The novel phosphor exhibits broad band near infrared emission with a maximum at 848 nm (FWHM = 140 nm at RT) that is assigned to the  $^4\text{T}_2 \rightarrow ^4\text{A}_2$  transition, characteristic for  $\text{Cr}^{3+}$  ions located in a low crystal field environment. The highest emission intensities were found for the sample doped with 15% of  $\text{Cr}^{3+}$ . The increasing concentration of  $\text{Cr}^{3+}$  causes a red shift of the emission band and was attributed to the presence of  $\text{Cr}^{3+}$  pairs. Temperature dependent measurements between 77 and 500 K showed rather low quenching temperature ( $T_{1/2} \approx 300 \text{ K}$ ) for the broad band  $\text{Cr}^{3+}$  emission due to the strong electron-phonon strength ( $S = 8$ ) and low energy position of the lowest  $^4\text{T}_2$  excited state. The  $\text{Sr}_8\text{MgLa}(\text{PO}_4)_7:\text{Cr}^{3+}$  phosphor shows excellent broad band NIR emission between 700 and 1000 nm but its application for high power broad band NIR pLEDs is limited by thermal quenching of the  $\text{Cr}^{3+}$  luminescence. In order to improve the thermal quenching behavior of  $^4\text{T}_2$  chromium emission in ortho-phosphates, one promising way would be a modification of the host composition through a solid solution with the same or at least similar crystal structure, i.e.  $(\text{Ba},\text{Sr},\text{Ca})_8(\text{Mg},\text{Zn})$

(La,Gd,Y,Lu)(PO<sub>4</sub>)<sub>7</sub>:Cr aimed at reducing the Stokes shift and shifting the emission maximum to slightly shorter wavelengths.

## Acknowledgement

The authors are grateful to Merz Pharmaceuticals GmbH for generous financial support.

## References

- [1] H.W. Siesler, Y. Ozaki, S. Kawata, H.M. Heise, Near-infrared Spectroscopy. Principles, Instruments, Application, Wiley-VCH Verlag, Weinheim, 2002.
- [2] M. Blanco, I. Villarroya, NIR spectroscopy: a rapid-response analytical tool, *Trends Anal. Chem.* 21 (2002) 240–250.
- [3] Y. Ozaki, Near-infrared spectroscopy - its versatility in analytical chemistry, *Anal. Sci.* 28 (2012) 545–563.
- [4] D. Hayashi, A.M. van Dongen, J. Boerekamp, S. Spoor, G. Lucassen, J. Schleipen, A broadband LED source in visible to short-wave-infrared wavelengths for spectral tumor diagnostics, *Appl. Phys. Lett.* 110 (2017) 233701.
- [5] C.J. Hayes, K.B. Walsh, C.V. Greensill, Light-emitting diodes as light sources for spectroscopy: sensitivity to temperature, *J. Near Infrared Spectrosc.* 25 (2017) 416–422.
- [6] OSRAM Opto Semiconductors, OSRON Black Series (850 Nm), SFH 4715S Data Sheet, Version 1.6, (Sept. 2016).
- [7] S. Möller, A. Katelnikovas, M. Haase, T. Jüstel, *J. Lumin.* 172 (2016) 185–190.
- [8] B. Malysa, T. Jüstel, D. Uhlich, I. Becker, H. Bettentrup, Infrared LED, German Patent DE102014107321 A1, 2015.
- [9] R.H. Mischeels, Solid State Broad Band Near-infrared Light Source, United States Patent No. 9528876 B2, (2016).
- [10] L. Zhang, S. Zhang, Z. Hao, X. Zhang, G.-H. Pan, Y. Luo, H. Wua, J. Zhang, A high efficiency broad-band near-infrared Ca<sub>2</sub>LuZr<sub>2</sub>Al<sub>3</sub>O<sub>12</sub>:Cr<sup>3+</sup> garnet phosphor for blue LED chips, *J. Mater. Chem. C* 6 (2018) 4967–4976.
- [11] C.-H. Huang, T.-M. Chen, Novel yellow-emitting Sr<sub>8</sub>MgLn(PO<sub>4</sub>)<sub>7</sub>:Eu<sup>2+</sup> (Ln = Y, La) phosphors for applications in white LEDs with excellent color rendering index, *Inorg. Chem.* 50 (2011) 5725–5730.
- [12] Z. Zheng, T. Wanjun, Tunable luminescence and energy transfer of Ce<sup>3+</sup>/Eu<sup>2+</sup>/Mn<sup>2+</sup>-tridoped Sr<sub>8</sub>MgLa(PO<sub>4</sub>)<sub>7</sub> phosphor for white light LEDs, *J. Alloy. Comp.* 663 (2016) 731–737.
- [13] R.D. Shannon, Revised effective ionic radii and systematic studies of interatomic distances in halides and chalcogenides, *Acta Crystallogr.* A32 (1976) 751–767.
- [14] M.G. Brik, Crystal field analysis, electron-phonon coupling and spectral band shape modeling in MgO:Cr<sup>3+</sup>, *Z. Naturforsch.* 60a (2005) 437–443.
- [15] P. Villars, K. Cenzual, Pearson's Crystal Data: Crystal Structure Database for Inorganic Compounds, ASM International®, Materials Park, Ohio, USA, 2017/18 Release.
- [16] C.-H. Huang, Y.-C. Chiu, Y.-T. Yeh, T.-S. Chan, T.-M. Chen, Eu<sup>2+</sup>-activated Sr<sub>8</sub>ZnSc(PO<sub>4</sub>)<sub>7</sub>: a novel near-ultraviolet converting yellow-emitting phosphor for white light-emitting diodes, *ACS Appl. Mater. Interfaces* 4 (2012) 6661–6668.
- [17] E. Nakazawa, F. Shiga, Vacuum ultraviolet luminescence-excitation spectra of RPO<sub>4</sub>:Eu<sup>3+</sup> (R = Y, La, Gd and Lu), *J. Lumin.* 15 (1977) 255–259.
- [18] H. Liang, Y. Tao, Q. Su, S. Wang, VUV-UV photoluminescence spectra of strontium orthophosphate doped with rare earth ions, *J. Solid State Chem.* 167 (2002) 435–440.
- [19] L. van Pieterson, A. Meijerink, Charge transfer luminescence of Yb<sup>3+</sup> in orthophosphates, *J. Alloy. Comp.* 300–301 (2000) 426–429.
- [20] H.H. Tjippins, Charge-transfer spectra of transition-metal ions in corundum, *Phys. Rev. B* 1 (1970) 126–135.
- [21] C.P. Poole, The optical spectra and color of chromium containing solids, *J. Phys. Chem. Solid.* 25 (1964) 1169–1182.
- [22] B. Malysa, A. Meijerink, W. Wu, T. Jüstel, On the influence of calcium substitution to the optical properties of Cr<sup>3+</sup> doped SrSc<sub>2</sub>O<sub>4</sub>, *J. Lumin.* 190 (2017) 234–241.
- [23] B. Malysa, A. Meijerink, T. Jüstel, Temperature dependent Cr<sup>3+</sup> photoluminescence in garnets of the type X<sub>3</sub>Sc<sub>2</sub>Ga<sub>3</sub>O<sub>12</sub> (X=Lu, Y, Gd, La), *J. Lumin.* 202 (2018) 523–531.
- [24] D.L. Wood, J. Ferguson, K. Knox, J.F. Dillon, Crystal-field spectra of d<sup>3,7</sup> ions. III. Spectrum of Cr<sup>3+</sup> in various octahedral crystal fields, *J. Chem. Phys.* 39 (1963) 890–898.
- [25] A. Patra, R.E. Tallman, B.A. Weinstein, Effect of crystal structure and dopant concentration on the luminescence of Cr<sup>3+</sup> in Al<sub>2</sub>O<sub>3</sub> nanocrystals, *Opt. Mater.* 27 (2005) 1396–1401.
- [26] C. Barthou, J. Benoit, P. Benalloul, A. Morell, Mn<sup>2+</sup> concentration effect on the optical properties of Zn<sub>2</sub>SiO<sub>4</sub>:Mn phosphors, *J. Electrochem. Soc.* 141 (1994) 524–528.
- [27] C.R. Ronda, T. Amrein, Evidence for exchange-induced luminescence in Zn<sub>2</sub>SiO<sub>4</sub>:Mn, *J. Lumin.* 69 (1996) 245–248.
- [28] B. Di Bartolo, Luminescence of Inorganic Solids, Plenum Press, New York, 1978.
- [29] B. Henderson, G.F. Imbusch, Optical Spectroscopy of Inorganic Solids, Oxford University Press, Oxford, 1989.
- [30] A.P. Vink, M.A. de Bruin, A. Meijerink, Line broadening studies for Cr<sup>3+</sup> pairs and single ions in different oxide lattices, *J. Phys. Condens. Matter* 12 (2000) 8607–8615.
- [31] D. Dragoman, M. Dragoman, Optical Characterization of Solids, Springer Verlag, Berlin, 2002.
- [32] A.P. Vink, M.A. de Bruin, S. Roke, P.S. Peijzel, A. Meijerink, Luminescence of exchange coupled pairs of transition metal ions, *J. Electrochem. Soc.* 148 (2001) E313–E320.
- [33] V. Bachmann, C. Ronda, A. Meijerink, Temperature quenching of yellow Ce<sup>3+</sup> luminescence in YAG:Ce, *Chem. Mater.* 21 (2009) 2077–2084.
- [34] R.C. Powell, Physics of Solid-state Laser Materials, Springer Verlag, New York, 1998.
- [35] Z. Zhang, K.T.V. Grattan, A.W. Palmer, Temperature dependences of fluorescence lifetimes in Cr<sup>3+</sup>-doped insulating crystals, *Phys. Rev. B* 48 (1993) 7772–7778.
- [36] T. Senden, R.J.A. van Dijk-Moes, A. Meijerink, Quenching of the red Mn<sup>4+</sup> luminescence in Mn<sup>4+</sup>-doped fluoride LED phosphors, *Light Sci. Appl.* 7 (2018) 8.